Available online at www.sciencedirect.com

ScienceDirect

IFAC Papers Online CONFERENCE PAPER ARCHIVE

IFAC PapersOnLine 56-2 (2023) 8242–8247

Finite Element Analysis of a High Compliant Balloon with Strain Sensing Segments for the Identification of Biomechanical Properties within Tubular Vessels

A. Bhave* B. Sittkus** S. J. Rupitsch*** U. Mescheder** K. Moeller*

*Institute of Technical Medicine, Furtwangen University, Germany. (Tel: +49 (0)7720-307-4785; e-mail: bha-furtwangen.de).

**Institute for Microsystem Technology, Furtwangen University, Germany (e-mail: siku@hs-furtwangen.de)

***Department of Microsystems Engineering, University Freiburg, Germany (e-mail: stefan.rupitsch@imtek.uni-freiburg.de)

Abstract: Conventional methods like Optical Coherence Tomography, Angiography, Fractional Flow Reduction, and Intravascular Ultrasound are used to identify stenosis within arterial vessel segments. These modalities are in fact not ideal to identify the diverse mechanical characteristics of the local tissue. To address the shortcomings, a strain sensing high compliant balloon system for tactile assessment of the vessel lumen is currently investigated in our groups. In this study, four exemplary balloon tissue interactions based on its corresponding 2D traverse cross section are simulated within a Finite Element Analysis (FEA). The simulations were analyzed in respect to the evolving strain states in 5 neighboring sensor elements along the balloon surface.

The conducted discussion evaluates the relevance of the obtained interdependencies in respect to an interpretation of the sensor segments, aiming at determining biomechanical properties of the surrounding vessel segment. Thereby, comparisons among the sensor segments and with respect to inflation sequences in the other vessel segments are discussed. Finally, relevant dependencies and design guidelines for strain sensing high compliant balloons are presented, paving the way for future refined FEA studies which ultimately aims for an intraoperative parameter identification with such high compliant sensor balloons.

Keywords: FEA, reverse identification, high compliant balloon, strain sensor, biomechanics, artery.

1. INTRODUCTION

Atherosclerosis, narrowing of vessels and calcification is reported in majority of patients suffering from coronary diseases and diseases of large or peripheral vessels. Angiography is the standard procedure to evaluate the thinning of vessel lumen and to decide on the intervention required to treat the narrowing (Wasserman et al., 2005). In conditions that are not severe, plaque formation causes arterial tissue remodeling and thickening of the artery wall while the lumen diameter remains its original shape and size. An angiograph is not able to provide information on the thickness of the vessels accurately nor on the tissue properties. This can underestimate the pathological nature of the arteries in question.

Imaging techniques like Intravascular Ultrasound (IVUS) and Optical Coherence Tomography (OCT) have shown moderate diagnostic accuracy for the detection of hemodynamically significant lesions (D'Ascenzo et al., 2015). OCT is reported to be at least 10 times higher in resolution compared to IVUS (10µm vs. 100µm). A drawback of OCT is that its penetration depth is 1–2 mm in comparison to IVUS' 5–6 mm. This leads to incomplete visualization of the vessel wall in large vessels, or in case of an increased plaque burden. (Kume et al., 2006; Sonoda et al., 2020) Studies propose that OCT may have a superior diagnostic accuracy in small vessels and IVUS is more suited for large vessels (D'Ascenzo et al., 2015; Sonoda et al., 2020). Recently, IVUS has been largely exploited in everyday clinical practice (Marteslo et al., 2020). FFR (Fractional Flow reserve) method can be used to determine the pressure drop across the stenosed vessels, thus, providing some partial information regarding the biomechanical properties of the vessel segments. However, this method cannot provide much information about localized tissue properties. (Bruyne & Sarma, 2008)

The above listed techniques are used to determine the choice of surgical intervention required by the vascular surgeon. Procedures like angioplasty, stenting, atherectomy are some of the well-known procedures performed. What is crucial to the success of the procedures is that the vessels do not undergo high plastic deformation or rupture during the procedure and that within the treated vessel segments high shear forces do not lead to an early restenosis due to new plaque formation (Hosokawa et al., 2015; Inami et al., 2015).

Factors like age, sex, pathology of tissue, location and degree of stenosis have shown to strongly influence the material properties, structural behavior and perfusion of the artery. The biomechanics of the tissue also show a large variability

Peer review under responsibility of International Federation of Automatic Control.
10.1016/j.ifacol.2023.10.1008

depending on collagen/ elastin composition of arteries. (Holzapfel et al., 2004; Kwak et al., 2014; Rossi et al., 2011). With the earlier mentioned techniques commonly used, the surgeons lack the important biomechanical data (with decision aids) that could possibly result in a more appropriate choice of intervention and better long-term outcome of the chosen procedure. The vascular surgeon would benefit from information on how much dilatation pressure leads to which values regarding maximum local stress and strains in the diseased vessel wall, what magnitude of shear force is introduced during the dilatation, how is the plaque distributing along circumferential direction and more general, what tissue biomechanics are present.

With a focus on providing such data intraoperatively with a high compliant diagnosis balloon catheter, two research institutes at Furtwangen University, namely Institute of Technical Medicine and Institute of Microsystems Technology are working on the development of an intra-luminal sensor-actuator setup that can provide local biomechanical properties of vessels and decision aids, in-vivo, during a clinical procedure (Sittkus et al., 2019; Sittkus et al., 2021). Investigations show how tissues may behave with partly stenosed tissue using 'fibre based' FEA models (Bhave & Möller, 2021a). Further studies of our group also show how deviating lumen profiles affect the local stretching of tissues in comparison to purely cylindrical structures (Bhave & Möller, 2021b). High compliant balloon interaction with different stiff tissue geometries has also been investigated and provides first insights to a tissue shape identification (Bhave et al., 2022).

The objective of the high compliant sensor-actuator balloon currently under development is the tactile assessment of the inner lumen wall of vessels in-vivo while providing shape and stiffness information. The strain sensing elements (based on microcracked ultrathin metal films) are being designed to be embedded inside the high compliant balloon wall relating obtained electrical resistance changes to the local deformation of the balloon. Compared to other sensor principles (e.g. capacitive), the resistive strain sensor principle is favored as it requires only a single "active" sensor layer and enables stable and easy readout circuitry for DC resistance measurements. To define requirements for the sensor elements (e.g., sensitivity and strain range), it is therefore necessary to study the interaction of high compliant elastomer-based balloons with healthy and pathological vessel segments with a focus on stretching induced to the sensor elements. This data can be used as design guideline for the sensor elements and their respective placement as well as for inverse, i.e., "reverse modelling" and "parameter identification" with later real sensor-equipped high compliant balloons.

2. METHODS

The current work aims at exploring a sensor-balloon interaction with 4 different types of vessel models based on available data of healthy and calcified/fibrosed artery segments. Thereby, the focus lies on the fibrosed segment identification with and without lumen occlusion by analyzing the circumferential stretch inside the balloon wall. We used the FEA-software COMSOL® (v6) to perform the FEA study and analysis. Four exemplary situations and its corresponding cross transverse sections where initialized as 2D simulations. The basis for the models (M(1)) was the expansion of the high compliant balloon without surrounding tissue. The different interaction scenarios refer to the contact with a healthy vessel segment (M(2)), a fully calcified vessel with no lumen narrowing (M(3)), with a partially calcified vessel and no lumen narrowing (M(4)), and partially calcified vessel with lumen narrowing (M(5)) (**Fig. 1**).

To observe the localized circumferential stretch in the balloon during expansion with idealized sensor elements, the outer circumference of the balloon was subdivided into 5 equal sections representing such sensor elements (S1 to S5 (M(2)) Fig. 1). The reference sensor length and the corresponding increasing length for a cylindrical expansion can then be calculated based on the angular sensor resolution θ defined by the sensor layout with

$$L_{Sx}(i) = 2\pi(r(i) + t_B(i))\frac{\theta}{360}, \quad (1)$$

where $L_{Sx}(i)$ is the inflation pressure dependent sensor length, $r(i)$ is the corresponding balloon radius and $t_B(i)$ is the balloon thickness.

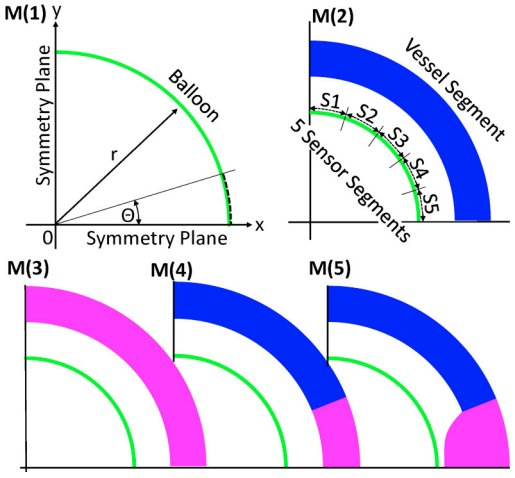

Fig. 1. FEA-Model setups for the different inflation sequences studied in the current work and the corresponding sensor segment definition. Green refers to the high compliant balloon, blue to healthy and magenta to calcified tissue segments.

The balloon and vessel components' mechanical behavior were initialized with experimentally validated models and their parameter values. The balloon material was initialized by a 4-term Ogden model for the elastomer Polydimethylsiloxane (PDMS) (Bernardi et al., 2017; Hopf et al., 2016), which was also used in first experiments of our group (Sittkus et al., 2019; Sittkus et al., 2021). The healthy part of the tissue was initialized with an exponential base model (Demiray, 1972) with values provided in (Delfino et al., 1997), whereas the calcification affected (pathological fibrosed) tissue was initialized using a 3 parameter Yeoh model (Yeoh, 1993). The values for the calcified tissue are provided in (Lawlor et al., 2011; Seime et al., 2022). All parameters are listed in **Table 1**.

The starting balloon thickness and radius for all the simulations measured 0.020 mm and 3 mm, respectively. The above dimensions were chosen for its appropriate circumferential perimeter that was smaller than the lumen perimeter of healthy or partly fibrosed medium sized arteries (Ota et al., 2005) and its manufacturability of the balloon. The geometry of vessels and distribution of healthy and calcified components were motivated from histological and structural analysis of vessels (Holzapfel & Ogden, 2010; Ota et al., 2005). In this study, these have been simplified to assess and correlate balloon deformation to clearly differentiable vessel structures. The vessel geometries for simulations M(2), M(3) and M(4) were initialized as an ideal transverse section of a cylinder (Fig. 1). The inner and outer radial dimensions were 4 mm and 5 mm, respectively, representing a category of medium sized arteries. The M(2) vessel was initialized with healthy tissue material properties; M(3) with completely calcified tissue properties; M(4) with approximately 75% healthy tissue and 25% area with calcified tissue properties. M(5) is initialized with partial lumen occlusion due to thicker calcified tissue occluding about 10 % of the lumen area.

Table 1. Parameters for utilized FEA material models

Model-Part (color)	Parameter [unit]	Value
high-compliant PDMS Balloon (green)	α_1	2.17
	α_2	9.06
	α_3	34.3
	α_4	-5.4
	μ_1 in MPa	2.91e-01
	μ_2 in MPa	3.40e-03
	μ_3 in MPa	2.01e-11
	μ_4 in MPa	-1.15e-02
	E in MPa	1.09
Healthy Tissue (blue)	D1 in kPa	2.645
	D2	8.36
Calcified Tissue (magenta)	C_{10} in kPa	302
	C_{20} in kPa	-228
	C_{30} in kPa	261

We simulated a quarter of the balloon and tissue with symmetric conditions about its x- and y-axes (Fig. 1). Pressure was applied to the inner surface of the balloon from 0 kPa to 10 kPa in steps of 0.5 kPa while the solver was able to choose free stepping for better convergence. The frictionless contact nodes of balloon and tissue were configured to be solved by the penalty method formulation, which allows slight overlapping at the contact boundary but decreases solving time. The balloon was meshed with mapped mesh elements leading to a total of 450 elements with an average element quality (skewness of the element) of ≈ 0.99. The tissues were also initialized with mapped mesh elements leading to an element count of 1152 (for M(2) to M(4)) with an average element quality of ≈ 0.97 and for setup M(5) with lumen occlusion to 1296 elements with an average element quality of ≈ 0.95. The ratio between the elements on the balloon boundary to the tissue boundary was set to be greater than a factor of 2. The resultant circumferential strain S_x of the individual sensors on the balloon for all the simulations is analyzed against the applied pressure.

To validate the results a mesh convergence analysis was conducted for all models. For an element count increase of factor 9 the maximum difference for S_x was 0.02 % in the model configuration M(5) with lumen occlusion.

3. RESULTS

In **Fig. 2**, the relative perimeter increase with increasing inflation pressure is shown for the free balloon inflation as well as for all model configuration in contact with the tissue. It clearly displays the deviating perimeter increase up to the maximum pressure applied. In **Fig. 3** (a), superimposed balloon inflation states are shown for the partly fibrosed lumen occluding model M(5) and in Fig. 3 (b), the final deformed states are shown for the different model setups M(2) to M(5).

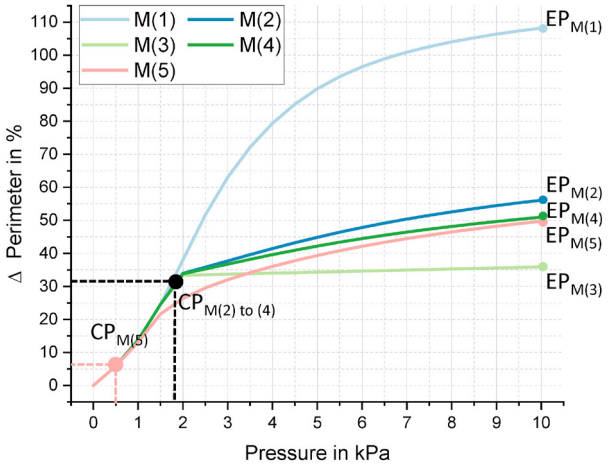

Fig. 2. Balloon perimeter pressure inflation of different model-setups. CP_{xx} thereby represents the initial Contact Point between balloon and tissue during inflation. EP_{xx} corresponds to the observed final states (End Points) in the current study. The perimeter is given as relative to the initial value corresponding to the commonly used engineering strain.

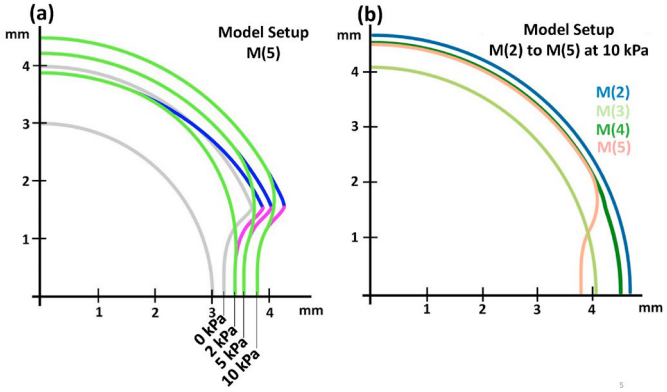

Fig. 3. Superimposed balloon inflation states for (a) M(5) at different inflation pressures and (b) all final deformed balloon states at the analysed maximum inflation pressure of 10 kPa. The shown states correspond to EPxx in Fig. 2.

In **Fig. 4** (a) and (b), a comparison between the relative perimeter expansions for different combinations is presented, with reference to the healthy tissue expansion in (a) or among the pathological changed vessel segments M(3) to M(5) in (b). **Fig. 5** and **Fig. 6** depict a comparison of engineering strain

levels for different sensor elements during an inflation sequence for the model setups M(4) and M(5), respectively. Further, the relative difference is plotted in correspondence to the right axis.

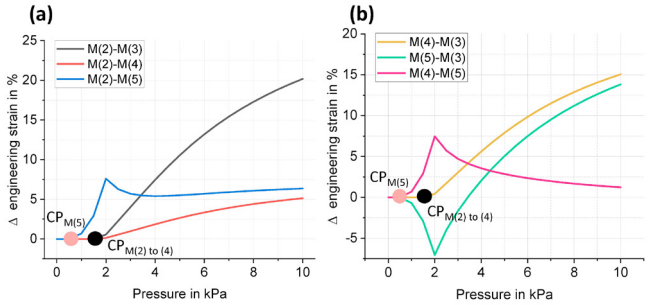

Fig. 4. Comparison between relative balloon perimeter expansion for different combinations. (a) With reference to the balloon expansion in healthy tissue. (b) Comparison among models with pathological vessel segments.

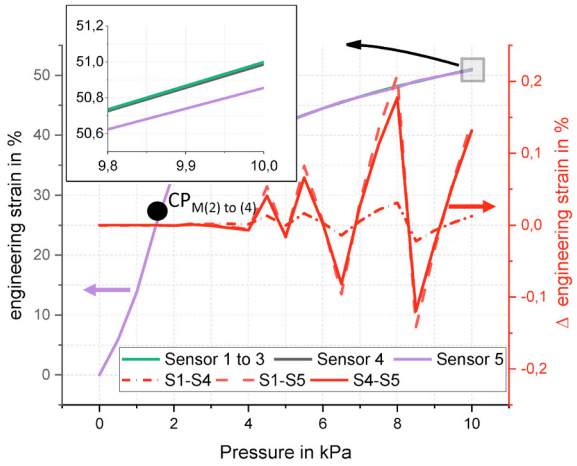

Fig. 5. Comparison of engineering strain levels among sensing elements S1 to S5 for the model setup M(4) with partially fibrosed tissue. Inset shows scaled maximum inflation area. Right axis represents the relative difference between chosen sensor segments.

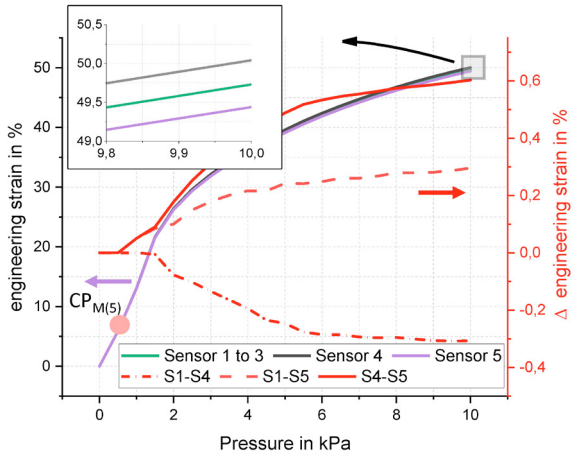

Fig. 6. Comparison of engineering strain levels between sensing elements S1 to S5 for the model setup M(5) with partially fibrosed lumen narrowing tissue. Inset shows scaled maximum inflation area. Right axis represents the relative difference between chosen sensor segments.

4. DISCUSSION

The exemplary situations are motivated by possible tissue structures encountered within pathological vessel segments of different grades. While they are not representative for real vessel cross sections, the tissue mechanics (healthy and calcified) are based on experimentally validated outputs from literature. Consequently, the following discussion aims for general relations, which pave the way for concretization and quantification within future refined models.

Looking at Fig. 2, it is obvious that the relative perimeter increase differs based on the encountered tissue state. Thereby, the perimeter increase can be tracked with a summation of each sensor element (S1 to S5). Neglecting the obvious difference between a free inflation and an inflation inside a vessel, the largest difference is obtained for an inflation within healthy (M(2)) vs. inside a fully fibrosed tissue (M(3)). The difference decreases for only partially fibrosed tissues (M(4) & M(5)). As the balloon is elastomer based and therefore high compliant, also the evolving balloon shapes largely differ from a cylindrical shape (Fig. 3), which would be retained by low compliant balloons, fulfilling only actuator purposes (e.g., common angioplasty balloons). As the motivation of this study is based on balloons for diagnostic purposes, this deviating shape can be utilized to differ between the different tissue stiffnesses and shapes.

Generally the sensors must be able to work within strain ranges up to or even larger than 100 %. Aiming solely for the differentiation between healthy and fibrosed tissue segment(s) only relatively low sensitivity is required. This can be ascribed to the fact that even for mildly and partially fibrosed vessel segments (M(2) – M(4)) without lumen narrowing, the obtained differences are above 1% (Fig. 4 (a)).

Complementing standard procedures, e.g., angiography in a meaningful way, requires quantitative assessments. For the targeted tactile assessment of vessels, it can generally be divided between biomechanical (e.g., stiffness) and geometrical vessel properties (e.g., (effective) diameter and circumferential spread of plaques). Regarding the accuracy of the obtained results, the sensor's sensitivity and the under in vivo conditions accessible signal to noise ratio (SNR) as well as the adaption of the balloon to the vessel lumen, viz., the balloon thickness and material as well as starting diameter (defining the stress state of the balloon wall at the initial CP), are the determining factors.

From the presented results, it is obvious that there are a multitude of signal analysis, which can be utilized for reverse identification. The initial contact (CP value) allows a vessel diameter evaluation or more precisely, the evaluation of the minimal cylindrical vessel diameter in the corresponding segment. Consequently, dependent on the angular sensor resolution, the differentiation between a lumen narrowing plaque or a pathological vessel wall degradation without spreading inside the vessel lumen (Fig. 4 (a) and (b)) can be distinguished. The subsequent slope of the evolving engineering strain (viz. the resistance correlate of the sensor) inside the individual sensor segments allows to determine the stiffness of the corresponding vessel segments, presupposing

that the contact maintains, and a suitable lumped model is chosen for the evaluation of such stiffness values (e.g. indentation correlates or if suitable, a simple subtraction of the balloon stiffness from the obtainable total stiffness). Hereby, it is important to note that nonlinearities of the balloon material, the tissue and possibly the sensor characteristics (if the resistance is not increasing linearly with the imposed strain) superimpose.

Aiming at a quantitative assessment of the plaque spread in circumferential direction, especially differing sensor segment responses can be utilized. Dependent on the pathological degradation (M(4) or M(5)), the necessary SNR and consequently the sensitivity of the sensor segments must be high as obtainable strain differences are < 1% (Fig. 5 and Fig. 6). For the performed simulations lumen narrowing plaques are easier to identify as induced evolving strain differences in the corresponding sensor segments are larger and lead to clear differences in the strain evolution (Fig. 6). For non-narrowing calcified segment, a clear separation between the strain evolution in the healthy part sensor segments and the calcified segments is not possible (Fig. 6). The obtainable circumferential resolution depends mainly on the angular sensor resolution (Fig. 1). Coevolving strain values (resistance values) of neighboring sensor segments can be interpreted as a contact with comparable tissue stiffnesses (e.g., healthy or fibrosed) and a smooth (e.g., cylindrical) lumen shape (compare Fig. 6 sensor 1 to 3).

For the reverse identification of the geometric lumen shape, the phase between an initial sensor segment deviation and the final contact state must be combined with a suitable lumped model of the interaction state. Here, it is important to note that information solely obtained from final states can lead to misinterpretations as strain (electrical resistance) values may coincide even the underlying (deformed) vessel geometry largely varies (e.g., M(4) and M(5) in Fig. 3 (b) and Fig. 4 (b)). This may happen even for a complete interpretation of the evolving strain values in respect to the inflation pressure. Consequently, the interpretation of sensor signals for unambiguously shape determination is for certain vessel states only possible with additional data. Despite the available angiograph, an easy to obtain parameter would be the utilized volume for the balloon inflation as with such, the two presented states in Fig. 3 (b) could be differentiated. Further, suitable datasets may be also reconstructed vessel geometries from dedicated imaging studies which then lead to certain sensor data interpretations based on the patient's status (e.g., age, sex, body size and weight, severity of symptoms).

With the current study results, it is possible to name certain dependencies and formulate some general design guidelines for strain sensing balloons:

- As reference for signal interpretation, a healthy tissue inflation reflecting a mean response based on the patient's status and region of intervention should be utilized.
- Coevolving strain states in neighboring sensor segments can be interpreted as a contact with comparable tissue mechanics and a (relative) regular lumen surface.
- Besides information stored in discrete strain states at certain inflation pressures, also the evolution of the same holds valuable information for a sensor data interpretation.
- Misinterpretations should be avoided by including additional available data to distinguish possibly coinciding strain states (and evolutions) in the balloon.
- For defined sensor layouts, the factors determining the accuracy of quantitative results are the balloon compliance and sensor sensitivity. Thereby, non-linearities superimpose and must be compensated.
- The required sensor sensitivity increases according to the targeted detection quantity. Based on an arbitrary reference sensitivity, the following sequence can be formulated, beginning with the lowest required sensitivity:
  1. Distinction healthy vs. pathological.
  2. Differentiating severe pathological states from early diseased states.
  3. Determining circumferential plaque spread in early diseased vessel segments with lumen narrowing.
  4. Detecting the circumferential calcified lumen while no lumen narrowing is present.

5. CONCLUSIONS

This study provides inputs for designing strain sensing diagnostic balloons while capturing limitations and challenges related with it. The balloon perimeter evolution can be utilized to differ between varying vessel pathologies while certain limitations must be considered. As starting point for parameter identification with lumped reverse modelling, some general interdependencies are concluded as well as some design guidelines for suitable sensor elements and layouts.

Addressing the limits of the current study, we will conduct further dynamic FEA based interaction studies, including frictional shear forces, viscoelasticity, Mullin's effect, differing sensor placements, tissue segments reflecting most encountered real pathological states and balloon movements relative to the tissue segments. This will lead to more interpretation possibilities of the obtained strain evolutions in sensor segments and ultimately to design rules for such sensor balloons. Addressing the transfer to clinical practice, we hope such cost-effective sensor balloons with a model based signal interpretation will pave the way to advanced and individual treatments leading to better long term outcomes of revascularizing therapies.

Author Statement

This research was partly supported by the German Federal Ministry of Research and Education (BMBF) under grant no. 13FH5I05IA (CoHMed/Digitalization in the OR) and under grant no. 2522FSB903-PerFluid (ERA PerMed).

REFERENCES

Bernardi, L., Hopf, R., Ferrari, A., Ehret, A. E. & Mazza, E. (2017) „On the large strain deformation behavior of silicone-based elastomers for biomedical applications“, *Polymer Testing*, Vol. 58, S. 189–198.

Bhave, A. & Möller, K. (2021a) „Analysis of expansion within a pressure inflated section of an urethral stricture

model“, *Current Directions in Biomedical Engineering*, Vol. 7, No. 2, S. 578–581.

Bhave, A. & Möller, K. (2021b) „Comparison of a histology based multi layer artery model to its simplified axisymmetric model“, *Current Directions in Biomedical Engineering*, Vol. 7, No. 2, S. 590–593.

Bhave, A., Rupitsch, S. J. & Moller, K. (2022) „Simulation study of inflation of a high compliant balloon inside idealized non-linear tissue geometry“, *Current Directions in Biomedical Engineering*, Vol. 8, No. 2, S. 672–675.

Bruyne, B. de & Sarma, J. (2008) „Fractional flow reserve: a review: invasive imaging“, *Heart (British Cardiac Society)*, Vol. 94, No. 7, S. 949–959.

D'Ascenzo, F., Barbero, U., Cerrato, E., Lipinski, M. J., Omedè, P., Montefusco, A., Taha, S., Naganuma, T., Reith, S., Voros, S., Latib, A., Gonzalo, N., Quadri, G., Colombo, A., Biondi-Zoccai, G., Escaned, J., Moretti, C. & Gaita, F. (2015) „Accuracy of intravascular ultrasound and optical coherence tomography in identifying functionally significant coronary stenosis according to vessel diameter: A meta-analysis of 2,581 patients and 2,807 lesions“, *American heart journal*, Vol. 169, No. 5, S. 663–673.

Delfino, A., Stergiopulos, N., Moore, J. E. & Meister, J. J. (1997) „Residual strain effects on the stress field in a thick wall finite element model of the human carotid bifurcation“, *Journal of biomechanics*, Vol. 30, No. 8, S. 777–786.

Demiray, H. (1972) „A note on the elasticity of soft biological tissues“, *Journal of biomechanics*, Vol. 5, No. 3, S. 309–311.

Holzapfel, G. A. & Ogden, R. W. (2010) „Constitutive modelling of arteries“, *Proceedings of the Royal Society A: Mathematical, Physical and Engineering Sciences*, Vol. 466, No. 2118, S. 1551–1597.

Holzapfel, G. A., Sommer, G. & Regitnig, P. (2004) „Anisotropic mechanical properties of tissue components in human atherosclerotic plaques“, *Journal of Biomechanical Engineering*, Vol. 126, No. 5, S. 657–665.

Hopf, R., Bernardi, L., Menze, J., Zündel, M., Mazza, E. & Ehret, A. E. (2016) „Experimental and theoretical analyses of the age-dependent large-strain behavior of Sylgard 184 (10:1) silicone elastomer“, *Journal of the mechanical behavior of biomedical materials*, Vol. 60, S. 425–437 [Online]. DOI: 10.1016/j.jmbbm.2016.02.022.

Hosokawa, K., Abe, K., Oi, K., Mukai, Y., Hirooka, Y. & Sunagawa, K. (2015) „Balloon pulmonary angioplasty-related complications and therapeutic strategy in patients with chronic thromboembolic pulmonary hypertension“, *International journal of cardiology*, Vol. 197, S. 224–226.

Inami, T., Kataoka, M., Shimura, N., Ishiguro, H., Yanagisawa, R., Kawakami, T., Fukuda, K., Yoshino, H. & Satoh, T. (2015) „Incidence, avoidance, and management of pulmonary artery injuries in percutaneous transluminal pulmonary angioplasty“, *International journal of cardiology*, Vol. 201, S. 35–37.

Kume, T., Akasaka, T., Kawamoto, T., Watanabe, N., Toyota, E., Neishi, Y., Sukmawan, R., Sadahira, Y. & Yoshida, K. (2006) „Assessment of coronary arterial plaque by optical coherence tomography“, *The American Journal of Cardiology*, Vol. 97, No. 8, S. 1172–1175.

Kwak, B. R., Bäck, M., Bochaton-Piallat, M.-L., Caligiuri, G., Daemen, M. J. A. P., Davies, P. F., Hoefer, I. E., Holvoet, P., Jo, H., Krams, R., Lehoux, S., Monaco, C., Steffens, S., Virmani, R., Weber, C., Wentzel, J. J. & Evans, P. C. (2014) „Biomechanical factors in atherosclerosis: mechanisms and clinical implications“, *European heart journal*, Vol. 35, No. 43, 3013-20, 3020a-3020d.

Lawlor, M. G., O'Donnell, M. R., O'Connell, B. M. & Walsh, M. T. (2011) „Experimental determination of circumferential properties of fresh carotid artery plaques“, *Journal of biomechanics*, Vol. 44, No. 9, S. 1709–1715.

Marteslo, J. P., Makary, M. S., Khabiri, H., Flanders, V. & Dowell, J. D. (2020) „Intravascular Ultrasound for the Peripheral Vasculature-Current Applications and New Horizons“, *Ultrasound in medicine & biology*, Vol. 46, No. 2, S. 216–224.

Ota, H., Takase, K., Rikimaru, H., Tsuboi, M., Yamada, T., Sato, A., Higano, S., Ishibashi, T. & Takahashi, S. (2005) „Quantitative Vascular Measurements in Arterial Occlusive Disease“, *RadioGraphics*, Vol. 25, No. 5, S. 1141–1158.

Rossi, P., Francès, Y., Kingwell, B. A. & Ahimastos, A. A. (2011) „Gender differences in artery wall biomechanical properties throughout life“, *Journal of hypertension*, Vol. 29, No. 6, S. 1023–1033.

Seime, T., van Wanrooij, M., Karlöf, E., Kronqvist, M., Johansson, S., Matic, L., Gasser, T. C. & Hedin, U. (2022) „Biomechanical Assessment of Macro-Calcification in Human Carotid Atherosclerosis and Its Impact on Smooth Muscle Cell Phenotype“, *Cells*, Vol. 11, No. 20.

Sittkus, B., Mescheder, U. M. & Urban, G. (2021) „Processing method of thin metal-polymer laminate membranes and transfer to cylindrically shaped substrates for flexible sensors“, in *MikroSystemTechnik Congress 2021*, S. 1–4.

Sittkus, B., Zhu, R. & Mescheder, U. (2019) „Flexible piezoresistive PDMS metal-thin-film sensor-concept for stiffness evaluation of soft tissues“, in *2019 IEEE International Conference 7/2019*, S. 1–3.

Sonoda, S., Hibi, K., Okura, H., Fujii, K., Honda, Y. & Kobayashi, Y. (2020) „Current clinical use of intravascular ultrasound imaging to guide percutaneous coronary interventions“, *Cardiovascular Intervention and Therapeutics*, Vol. 35, No. 1, S. 30–36 [Online]. DOI: 10.1007/s12928-019-00603-y.

Wasserman, B. A., Wityk, R. J., Trout, H. H. & Virmani, R. (2005) „Low-grade carotid stenosis: looking beyond the lumen with MRI“, *Stroke*, Vol. 36, No. 11, S. 2504–2513.

Yeoh, O. H. (1993) „Some Forms of the Strain Energy Function for Rubber“, *Rubber Chemistry and Technology*, Vol. 66, No. 5, S. 754–771.